European Journal of Remote Sensing - 2016, 49: 917-932
doi: 10.5721/EuJRS20164948
Received 30/01/2016 accepted 02/09/2016

European Journal of Remote Sensing
An official journal of the Italian Society of Remote Sensing

www.aitjournal.com

High rate GNSS measurements for detecting non-hydrostatic surface wave. Application to tidal borein the Garonne River

Frédéric Frappart[1,2]*, Nicolas Roussel[1], José Darrozes[1], Philippe Bonneton[3], Natalie Bonneton[3], Guillaume Detandt[3], Félix Perosanz[1,4] and Sylvain Loyer[5]

[1]Géosciences Environnement Toulouse (GET), UMR 5563, CNRS/IRD/UPS, Observatoire Midi-Pyrénées (OMP), Groupe de Recherche en Géodésie Spatiale (GRGS), 31400, Toulouse, France
[2]Laboratoire d'Etudes en Géophysique et Océanographie Spatiales (LEGOS), UMR 5566, CNES/ CNRS/IRD/UPS, Observatoire Midi-Pyrénées (OMP), Groupe de Recherche en Géodésie Spatiale (GRGS), 31400, Toulouse, France
[3]Environnements et Paléo-environnements Océaniques et Continentaux (EPOC), UMR 5805, CNRS/ Université de Bordeaux, Observatoire Aquitain des Sciences de l'Univers (OASU), 33615, Pessac, France
[4]Centre National d'Etudes Spatiales (CNES), 18 Avenue Edouard Belin, 31400, Toulouse, France
[5]Collecte Localisation Satellites (CLS), 31520, Ramonville Saint-Agne, France
*Corresponding author, e-mail address: frederic.frappart@legos.obs-mip.fr

Abstract
This study presents the results of the use of high frequency Global Navigation Satellites Systems (GNSS) data for the detection and the characterization of tidal bores. The experiment took place the 31st of August 2015 in the Garonne River, at 126 km upstream the mouth of the Gironde estuary. The GNSS data acquired on a buoy at a sampling rate of 20 Hz were processed with a differential GNSS technique using the RTKLIB freeware. GNSS-based elevation of the free surface provides accurate estimates of the tidal bore first wave amplitude (1.34 m) and period (3.0 s). These values were in good agreement with values obtained using ADCP measurements.

Keywords: Tidal bore, GNSS, high frequency, non-hydrostatic.

Introduction
GNSS provides autonomous geo-spatial positioning with global coverage thanks to more than 50 satellites from different constellations (the American Global Positioning System GPS, the Russian GLObalnaïa NAvigatsionnaïa Sistéma GLONASS, the European system Galileo, ...) emitting continuously L-band microwave signals.GNSS receivers on buoy are commonly used in tsunami warning systems [e.g., Yamagiwa et al., 2006; Falck et al., 2010], for the calibration of radar altimetry mission [e.g., Bonnefond et al., 2015; Frappart et al., 2015], sea surface monitoring [e.g., Bouin et al., 2009; Fund et al., 2013], swell and waves detection [e.g., Bender III et al., 2010], river stage monitoring [e.g., Apel et al., 2011]. In most applications using GNSS data, the acquisition rate is lower than or equal to

1 Hz. Recent studies showed the interest of using higher than 1 Hz sampling frequencies for seismic applications [e.g., Elósegui et al., 2006; Avallone et al., 2011, 2012].
Tidal bores in estuaries are small-scale (typically few seconds in time and dozen meters in space) highly complex estuarine processes which can form at the leading edge of flood tides. They generally occur in the upper estuary and result from the nonlinear transformation of the tidal wave over long distance (several dozen of kilometers) and long period of time (several hours) [Bonneton et al., 2015]. During the last 10 years, several quantitative field studies have contributed to a better understanding of wave, turbulent, and sediment processes associated with tidal bore propagation up river [Simpson et al., 2004; Wolanski et al., 2004; Uncles et al., 2006; Bonneton et al., 2011, 2012, 2015; Chanson et al., 2011; Furgerot et al., 2013]. These studies are based on the use of gauges records, pressure data and few Acoustic Doppler Current Profiler (ADCP) measurements to characterize tidal bores dynamics. None of them already used GNSS data for this purpose.
In this study, for the first time, GNSS data, acquired at a frequency of 20 Hz by a geodetic receiver in a buoy, were used as a new source of information to study the tidal bore that occurred on the 31st of August 2015 in the Gironde/Garonne estuary. We analyzed the spatio-temporal variations of GNSS positions acquired at high frequency (20 Hz) by a receiver on a buoy during a tidal bore that occurred in the Garonne River (France) in August 2015. We first describe the experimental set up and the datasets used here. We present then the technique used to process the GNSS data, and finally the results obtained during this field campaign.

Introduction

Study area

The Gironde estuary is located in the Bay of Biscay, on the southwest coast of France. It is formed by the confluence of the Dordogne and Garonne Rivers (Figs. 1a and b). The estuary has a funnel-shaped opening to the Bay of Biscay and a length of about 75 km. During spring tide, the tidal range at the estuary mouth can exceed 5 m. Large amplitude tidal waves propagate into the Garonne and Dordogne rivers up to 160 km from the estuary mouth. Tidal bores, up to 1.5 m high, can form in both the Garonne and the Dordogne Rivers [Bonneton et al., 2012]. Field experiments were carried out in the Garonne River at Podensac, 126 km upstream the river mouth. This site was selected owing to the presence, during spring tide, of well-developed undular tidal bores and also because the absence of any significant curvature of the river at this location limits the complexity of the tidal bore dynamics [Bonneton et al., 2011, 2012, 2015]. A detailed bathymetric survey of 1 km long was previously conducted at the study site, in Podensac, at the beginning of the 2010 and 2011 campaigns [Bonneton et al., 2015]. The cross-sectional river width is 150 m, and the side bank slopes on the right and left banks are, respectively, around 35% and 10%. These experiments were carried out during spring tide and for low freshwater discharges. For such conditions tidal bores can form at the beginning of the rising tide. The mean bore intensity can be characterized by the Froude number (*Fr*):

$$Fr = \frac{|u_1 - c_b|}{(gD_1)^{1/2}} \quad [1]$$

where u_1 and D_1 are the cross-sectionally averaged velocity and water depth ahead the mean jump (*i.e.*, primary wave) respectively, g is the gravitational acceleration, and c_b is the bore celerity. More details about the tidal bore dynamics in the Gironde/Garonne estuary can be found in Bonneton et al. [2015].

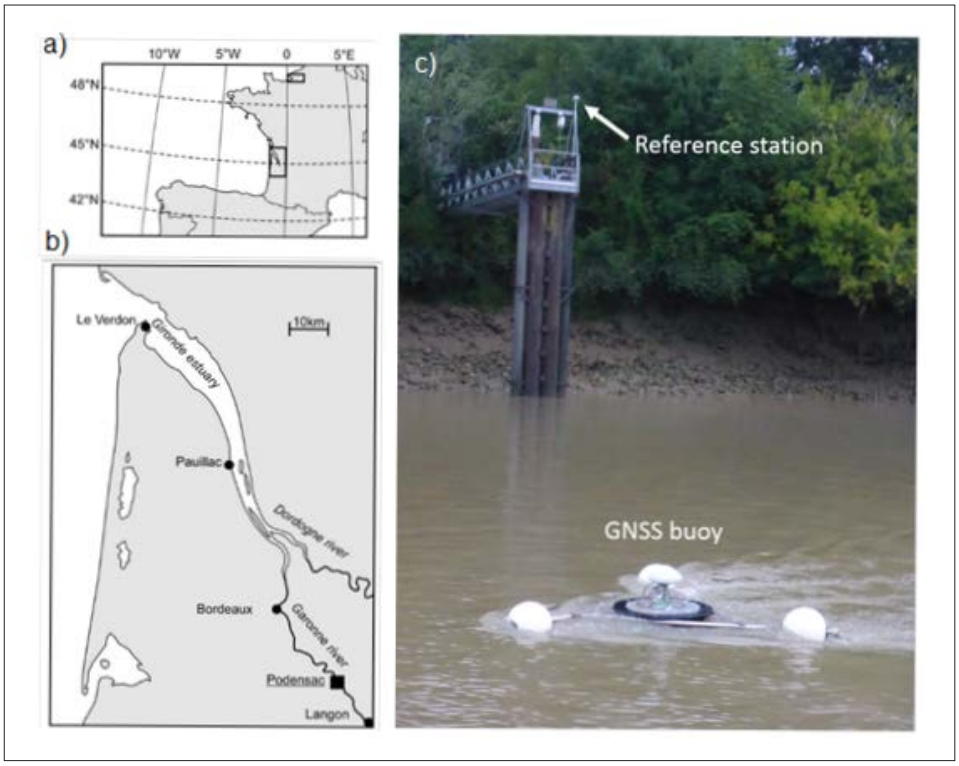

Figure 1 - The Gironde estuary is located in the southwest of France (a). It is formed by the confluence of the Garonne and the Dordogne rivers, upstream Bordeaux. The Podensac study site is located on the Garonne River, at 126 km from the mouth of the Gironde estuary (b). Our experimental setup was composed of two GNSS receivers with their antenna located on a platform (reference station) and on a buoy, completed by a pressure and an ADCP (not visible on this picture) (c).

GNSS data

Two GNSS geodetic stations were installed during this field campaign: one on a buoy used as a rover for monitoring the changes affecting the river surface and another one on a platform a few meters away from the buoy (or rover) and used as a base station (see Fig. 1c). The two GNSS stations are composed of Leica GR25 receivers and AR10 antennae. They operate at multi-frequencies (L1, L2, L5) on multi-constellation signals. They were acquiring GNSS (GPS and GLONASS) data at a sampling rate of 0.05 s or 20 Hz between 17h and 17h23 UTC on 31st of August 2015. The base station on the platform also acquired GNSS data at a sampling rate of 1 s (1 Hz) from 13h56 UTC on 31st of August 2015 to 13h32 UTC on 2nd of September 2015.

GNSS records from La Brède (LBRD) station (from Réseau GNSS Permanent (RGP, http://rgp.ign.fr/), a permanent network of GNSS stations in France operated by Institut National de l'Information Géographique et Forestière (IGN), were also used to estimate possible changes in elevation of the platform on which was set the base station during the tidal cycle, and especially during the tidal bore. This station, an ASHTECH ProFlex500 receiver with a Navcom 3001 antenna, operating at two frequencies (L1 and L2) on GPS and GLONASS signals, is located at (00° 31' 40.16951" W, 44° 40' 53.11627" N, 72.560 m) in the French geodetic system (Réseau Géodésique Français 1993 - RGF93), at 14.57 km from the base station.
Satellite coordinates product providing GNSS orbit and clock offset data (GNSS day 18601) used in this study were made available by the International GNSS Service (IGS) at ftp://cddis.gsfc.nasa.gov/gps/products/. We chose the product from Groupe de Recherche en Géodésie Spatiale (GRGS - http://grgs.obs-mip.fr/). It contains precise ephemeris in the SP3 format and clock final products with a temporal resolution of 15 min for both GPS and GLONASS. We also used the Antenna Exchange Format (ANTEX) file (igs08_wwww.atx), made available by IGS (https://igscb.jpl.nasa.gov/igscb/station/general/igs08.atx) that provides precise and consistent set of phase center offset (PCO) and variation (PCV) values for both satellites and receivers antennae. The PCO is the difference between the antenna reference point (ARP) and the mean phase center, whereas the PCV values provide additional zenith- and/or azimuth-dependent corrections that defines the phase pattern (individually for each carrier frequency) to get the actual phase center position [Hofmann-Wellenhof et al., 2008]. More details about the ANTEX file can be found in Montenbruck et al. [2015].

Pressure and acoustic surface water elevation datasets

Continuous water elevation measurements were carried out with two different methods. The first one is based on classical pressure measurements, with a sampling frequency of 10 Hz. The second one relies on direct acoustic surface tracking measurements (Signature 1000 Khz, Nortek ADCP) with a sampling frequency of 8 Hz.

GNSS data processing

The DGNSS technique

The GNSS carrier phase emitted by a satellite k at the wavelength λ and observed by a receiver i equals [Hofmann-Wellenhof et al., 2008]:

$$\lambda\Phi_i^\kappa(t_\varepsilon,t_\rho) = \rho_i^\kappa(t_\varepsilon,t_\rho) - c(\delta\tau_\rho - \delta\tau_\kappa) + \lambda N_i^\kappa + \delta_{\iota\sigma\nu} + \delta_{\tau\rho\sigma\pi} + \delta_{\tau\iota\delta\varepsilon} + \delta_{\rho\varepsilon\lambda} + \varepsilon_\pi \quad [2]$$

where is the range between the receiver i and the satellite k, t_e and t_r are the GNSS emission time for satellite k and the GNSS reception time for receiver i respectively, c is the speed of light in the vacuum, δt_r and δt_k are the clock errors of the receiver and the satellite at the time t_r and t_e respectively, is the carrier phase ambiguity for the receiver i and the satellite k, δ_{ion}, δ_{trop}, δ_{tide} and δ_{rel} are the ionospheric, tropospheric, tidal (including solid Earth, pole and ocean loading tides) and relativistic effects respectively, and ε_p is the remaining error on the phase including errors due to multipaths.
The DGNSS technique consists in computing very accurately the position of a GNSS station assumed to be fixed (*i.e.*, the base station) and then estimating the position of the second receiver (*i.e.*, the mobile or the rover), generally varying against time, with reference to the

base computing single or double differences for every GNSS satellite from both stations (*i.e.*, the base i_1 and the rover i_2). Single difference (SD) is the difference formed by data observed (O) at two stations on the same satellite at epoch t [Hofmann-Wellenhof et al., 2008]:

$$SD_{i_1,i_2}^{k}(t) = O_{i_2}^{k}(t) - O_{i_1}^{k}(t) \quad [3]$$

Applied to the GNSS carrier phase from [2], [3] becomes:

$$\lambda\Phi_{i_2}^{k}\left(t_e,t_{r_2}\right) - \lambda\Phi_{i_1}^{k}\left(t_e,t_{r_1}\right) = \rho_{i_2}^{k}\left(t_e,t_{r_2}\right) - \rho_{i_1}^{k}\left(t_e,t_{r_1}\right) - c\left(\delta t_{r_2} - \delta t_{r_1}\right) + \lambda\left(N_{i_2}^{k} - N_{i_1}^{k}\right) + d\delta_{ion} + d\delta_{trop} + d\delta_{tide} + d\delta_{rel} + d\varepsilon_p \quad [4]$$

where $d\delta_{ion}$ and $d\delta_{trop}$ are the differenced ionospheric and tropospheric effects at the two stations related to the satellite k respectively, and $d\varepsilon_p$ is the remaining error on the phase.
In the case of very short baseline as in our experimental setup where the maximum distance between the two stations is lower than 20 m, we can consider that the atmosphere effects are the same. So, [4] can be simplified as follows:

$$\lambda\Phi_{i_2}^{k}\left(t_e,t_{r_2}\right) - \lambda\Phi_{i_1}^{k}\left(t_e,t_{r_1}\right) = \rho_{i_2}^{k}\left(t_e,t_{r_2}\right) - \rho_{i_1}^{k}\left(t_e,t_{r_1}\right) - c\left(\delta t_{r_2} - \delta t_{r_1}\right) + \lambda\left(N_{i_2}^{k} - N_{i_1}^{k}\right) + d\varepsilon_p \quad [5]$$

Doubles differences are the combination of two single differences. They can be considered as between-satellite single differences of between-receiver single differences. Double difference (DD) is the difference formed by SD at two stations for two satellites k_1 and k_2 [Hofmann-Wellenhof et al., 2008]:

$$DD_{i_1,i_2}^{k_1,k_2}(t) = SD_{i_1,i_2}^{k_2}(t) - SD_{i_1,i_2}^{k_1}(t) \quad [6]$$

$$DD_{i_1,i_2}^{k_1,k_2}(t) = \rho_{i_2}^{k_2}\left(t_e,t_{r_2}\right) - \rho_{i_1}^{k_2}\left(t_e,t_{r_1}\right) - \left(\rho_{i_2}^{k_1}\left(t_e,t_{r_2}\right) - \rho_{i_1}^{k_1}\left(t_e,t_{r_1}\right)\right) + \lambda\left(N_{i_2}^{k_2} - N_{i_1}^{k_2} - N_{i_2}^{k_1} + N_{i_1}^{k_1}\right) + d\varepsilon_p \quad [7]$$

They permit to estimate the integer ambiguities independently of the clock bias [Petrovello, 2011].
Finally, triple differences (TD) can be considered by differencing the DD between two consecutive epochs t^n and t^{n+1}[Hofmann-Wellenhof et al., 2008].

$$TD_{i_1,i_2}^{k_1,k_2}(t^n,t^{n+1}) = DD_{i_1,i_2}^{k_1,k_2}(t^n) - DD_{i_1,i_2}^{k_1,k_2}(t^{n+1}) \quad [8]$$

$$TD_{i_1,i_2}^{k_1,k_2}(t^n,t^{n+1}) = \rho_{i_2}^{k_2}\left(t_e^{n+1},t_{r_2}^{n+1}\right) - \rho_{i_1}^{k_2}\left(t_e^{n+1},t_{r_1}^{n+1}\right) - \left(\rho_{i_2}^{k_1}\left(t_e^{n+1},t_{r_2}^{n+1}\right) - \rho_{i_1}^{k_1}\left(t_e^{n+1},t_{r_1}^{n+1}\right)\right) - \left(\rho_{i_2}^{k_2}\left(t_e^{n},t_{r_2}^{n}\right) - \rho_{i_1}^{k_2}\left(t_e^{n},t_{r_2}^{n}\right) - \left(\rho_{i_2}^{k_1}\left(t_e^{n},t_{r_2}^{n}\right) - \rho_{i_1}^{k_1}\left(t_e^{n},t_{r_1}^{n}\right)\right)\right) + d\varepsilon_p \quad [9]$$

They cancel the effect of ambiguities allowing the determination of GNSS solutions without considering them [Remondi, 1985].

GNSS data processing

GNSS raw data were processed using the RTK open source program package [Takasu, 2009; Takasu and Yasuda, 2009]. This freeware is available at: http://www.rtklib.com/. We used the latest version available (version 2.4.2) of the RTKLIB software. As mentioned above, a DGNSS approach was applied for processing the data of the GNSS station in the buoy acquired at a sampling frequency of 20 Hz with reference to the data from the base station due to the very short baseline between the two stations and the small length of the acquisition period. We also checked if the platform was affected by changes in elevation due to the tide and the tidal bore. We performed a DGNSS processing on the Podensac base station acquired at 1 Hz using La Brède station from RGP as a base station. Same positioning mode (DGNSS) was chosen and same corrections were applied for the processing of the GNSS data using RTKLIB at both sampling frequencies. Figure 2 presents the visibility of the GNSS satellites for the three receivers used in this study between 17h00 UTC and 18h00 UTC on the 31st of August 2015. We can see that the three GNSS antennae acquired signals at least L1 and L2 frequency bands most of the time. This is the case for all the observation period. So, the data were processed using L1 and L2 phase carrier observations, using Saastamoinen model for correcting the tropospheric effects, in ionosphere-free mode, and applying solid Earth and pole tides, and ocean tide loading. The data were processed in static and kinematic modes in the cases of the Podensac base station (1 Hz) and of the buoy (20 Hz) respectively. Using the Saastamoinen model, δ_{trop} is expressed in meters as follows [Saastamoinen, 1973]:

$$\delta_{trop} = \frac{0.002277}{cos(z)}\left[p + \left(\frac{1255}{T} + 0.05\right)e - tan^2(z)\right] \quad [10]$$

where z is the zenith angle of the satellite, p is the surface atmospheric pressure (mbar), T is the surface air temperature (K), e is the surface partial pressure of water vapor (mbar).
Availability of L1 and L2 carrier phase observations allow the use of the ionosphere free mode that permits to eliminate the ionosphere delay by using two signals of different frequencies [Hofmann-Wellenhof et al., 2008]. Using a linear combination of [2] for L1 and L2 frequencies (f_1 and f_2 respectively), we finally obtained:

$$\Phi_c = \frac{f_1^2}{f_1^2 - f_2^2}\left(\Phi_1 - \frac{f_2}{f_1}\Phi_2\right) = \frac{f_1^2\rho_i^k(t_e,t_r,f_1) - f_2^2\rho_i^k(t_e,t_r,f_2) + \lambda_1 N_i^k(f_1) - \lambda_2 N_i^k(f_2) + \delta_{tropo}(f_1) - \delta_{tropo}(f_2) + \varepsilon_p(f_1) + \varepsilon_p(f_2)}{f_1^2 - f_2^2} \quad [11]$$

This new carrier phase observable (Φ_c), in which the ionosphere delay is eliminated (practically, it is reduced), will be used for processing the GNSS and estimate the position of the GNSS antennae.
Solid Earth and pole tides, and ocean tide loading corrections follow the IERS Conventions [2010].

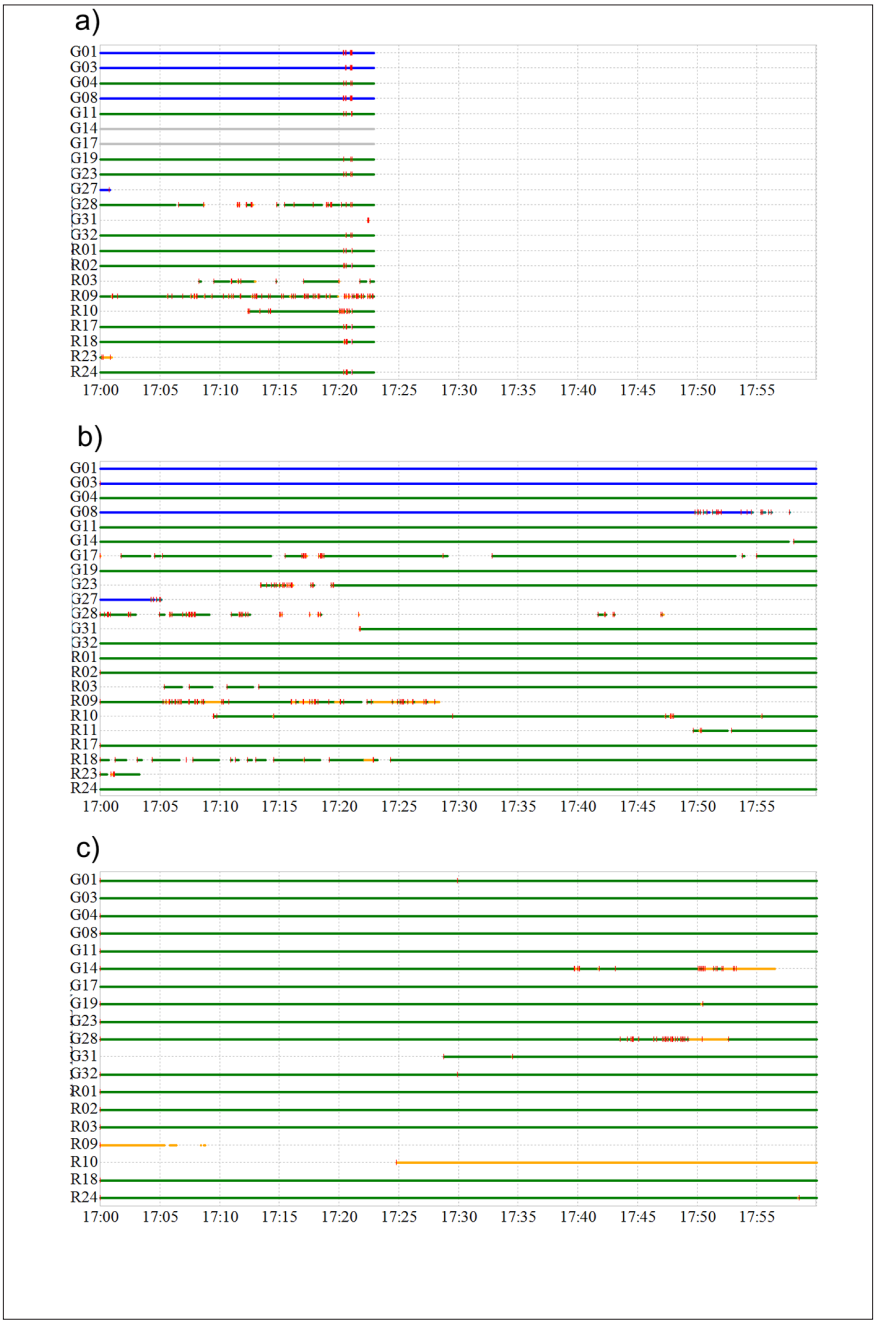

Figure 2 - GNSS satellites visibility on the 31st of August 2015 from 17h00 to 18:00 UTC at Podensac on the buoy (a), at the base station (b) and at La Brède RGP station (c). The color of the lines corresponds to the frequencies of the GNSS observations: L1 (orange), L1/L2 (green), L1/L2/L5 (blue), L5 (grey). Small red vertical lines correspond to acquisition losses.

Results

Possible effect of the tides on the height of the base station

The base station, that was used as reference in the processing of the GNSS data acquired at 20 Hz on the buoy, was mounted on the platform. We wondered if the platform, and so the GNSS antenna, were affected by the tidal cycle and if the signature of the tidal bore can be detected on the GNSS records. We processed the GNSS data acquired at 1 Hz on the 31st of August 2015 using a classical DGNSS processing using the RGP station LBRD located in La Brède, at 14.57 km from the Podensac study site, as reference. As the number of visible GNSS (GPS and GLONASS) satellites is never lower than 14, and as most of the observations are acquired at L1 and L2 bands for both stations (Fig. 2), static positioning was performed in iono free mode using the following parameters for processing the data: resolution of the integer ambiguity in "continuous" mode, elevation mask of 10°, "outage to reset ambiguity" of 3, "slip threshold" of 0.1 m, "reject threshold of GDOP" of 3 and "innovation" of 0.5 m. Standard deviations are 0.06, 0.01 and 0.01 m on the x, y and z components respectively when only using satellites measurement from the GPS constellation. Similar results are obtained using only the GLONASS constellation or combining measurements from both constellations, with a slight improvement on the x component (0.05 and 0.04 m of std for GLONASS and GPS + GLONASS respectively). The platform is hence not affected by tides that present a dominant semi-diurnal (6h) component in the Gironde estuary and the Garonne River. No supplementary correction due to changes in height of the base station needs to be taken into account when analyzing the data acquired by the GNSS receiver in the buoy.

Detection of the tidal bore and validation of GNSS estimates of the variations of the free surface elevation

The estimates of the vertical position of the GNSS antenna (h) were compared to measurements of the free surface elevation acquired by the ADCP during the tidal bore passage. These estimates were obtained using a kinematic DGNSS processing of the 20 Hz data (see 3.2 GNSS data processing) applied to GPS and GPS + GLONASS data. Due to the small number of GLONASS satellites visible between 17h00 and 17h25 (5, all of them not visible by the receiver on buoy at different epochs - see Fig. 2a), RTKLIB was unable to retrieve the buoy position only based on GLONASS data. Comparisons between GPS and GPS + GLONASS retrievals of the buoy position were performed. They showed a very high consistency the one another with RMSE lower than 0.005 m on every component. They also exhibited low variability in the free surface height before the first tidal bore wave with std of the water stage (z component) equals to 0.008 and 0.005 m for GPS, and GPS + GLONASS solutions respectively during the first 7.5 s of acquisitions presented in Fig. 3 (and equals to 0.003 m for the first 5 s). The stability of the solutions was obtained for a wide range of parameters used for processing the data: resolution of the integer ambiguity in "fix and hold" and "continuous" modes, elevation mask between 5 and 10°, "outage to reset ambiguity" ranging from 3 to 5, "slip threshold" from 0.05 to 0.1 m, "reject threshold of GDOP" above 5 and "innovation" above 2 m.

The GNSS antenna is on a buoy whereas the ADCP location is fixed. To be compared, the GNSS estimates had to be corrected for an advection term using the following Equation:

$$\frac{Dh}{Dt} = \frac{\delta h}{\delta t} + \vec{c}_b \cdot \vec{\nabla} h \quad [12]$$

where $\frac{Dh}{Dt}$ is the Lagrangian derivative of h, $\frac{\delta h}{\delta t}$ its partial derivative against, $\vec{c}_b$ is the wave celerity, and $\vec{\nabla} h$ is the gradient of h. The wave celerity c_b was estimated to be 5.2 ms^{-1}. Considering this celerity constant during the tidal bore, we shifted the time to account for the displacement of the buoy as follows:

$$t_{GNSS}^{shift} = t_{GNSS} - \frac{\sqrt{\left(x(t) - x(t_0)\right)^2 + \left(y(t) - y(t_0)\right)^2}}{c_b} \quad [13]$$

where t_{GNSS}^{shift} is the time in a referential where the GNSS antenna is fixed, t_{GNSS} is the time of the GNSS receiver, x and y refer to the horizontal components of the position of the GNSS antenna on the buoy at time t, t_0 is the origin of the time.

Figure 3 presents a well-developed undular bore with a Froude number of 1.28, that started at 17h19mn45s on the 31st of August 2015. At the wave front passage, the elevation increases abruptly by 1.34 m in 3 s. The secondary wave field (also named whelps) associated with the front is characterized by a period of 3.0 s and a wave height (first wave) of 0.86 m. After 4 waves, the buoy started to sink.

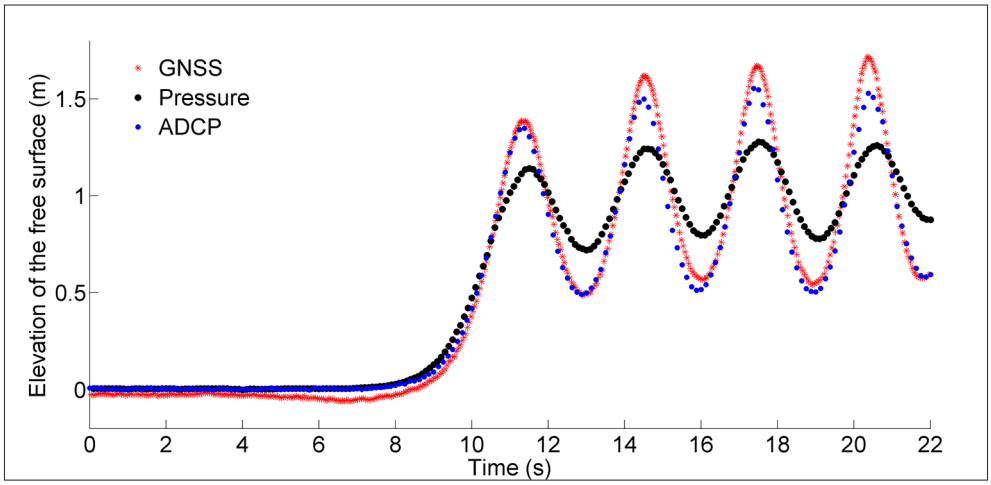

Figure 3 - Time variations of the free surface elevation as measured by GNSS (red stars), pressure sensor (black dots) and ADCP (blue dots). The origin of time was set at 17h19mn45s.

These results were compared to pressure and ADCP measurements. The wave height is strongly underestimated when the surface elevation is reconstructed from pressure measurements and the hydrostatic hypothesis (Fig. 3). This is in agreement with previous observations by Bonneton et al. [2015] that show that a non-hydrostatic reconstruction is required for a correct elevation estimation of well-developed undular bores from pressure

measurements. On the contrary, a very good agreement was found with ADCP measurements, especially for the first wave. For the following waves, changes in amplitudes up to 0.1 m for the extreme values were found. GNSS-based river stage also exhibit a slight decrease (starting at 5 s and reaching a maximum difference of 3 cm with ADCP measurement at 7.5 s - see on Fig. 3). The tidal bore waves, with their period of 3 s, were changing the attitude of the buoy causing variations in the center of phase of the antenna. These variations were not accounted for in the data and can explain the differences observed on Figure 3. The geometry of the buoy can be sketched as an equilateral triangular with sides of d=1.5 m long with the GNSS antenna at its center (see Figure 1). For simplification, we assumed that the tidal bore wave is perpendicular to one its side. Using the Thales (or intercept) theorem, the elevation of one of its vertex of a height dh caused an elevation of the center of the triangle where the antenna is located of $\sqrt{3}/3\ dh$. Taking into account, the wave celerity of the tidal bore (5.2 m.s^{-1}) and the distance between the center and the vertexes of the buoy (~0.87 m), the changes in time (dt) to be considered for estimating dh are ~ 0.17 s, that is roughly the sampling period of the ADCP measurements (8 Hz or 0.125 s). Changes in elevation of the free surface from ADCP measurements are presented in Figure 4. They are lower or equal to 0.15 m. If we consider dh_{max}=0.2 m to account for the shorter time sampling of the ADCP, the maximum difference of height with the smooth surface is 0.12 m, that was roughly observed on Figure 3. Similarly, a dh of 0.01 - 0.02 m around 7.5 - 8.5 s caused the decrease in river surface height of 0.005 - 0.01 m observed before the first wave of the tidal bore.

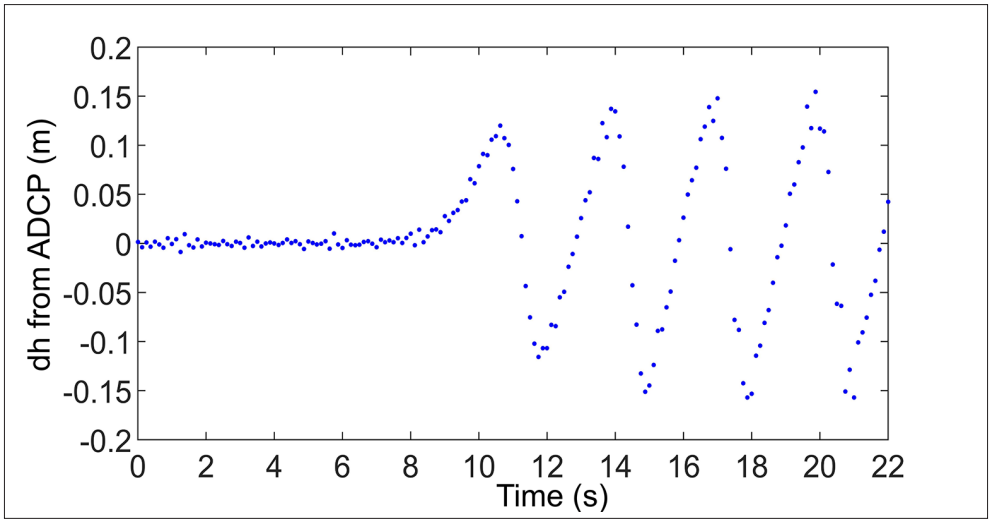

Figure 4 - Time variations of the changes in free surface elevation as measured by ADCP (blue dots). The origin of time was set at 17h19mn45s.

Time variations of the buoy horizontal position and velocity during the tidal bore

Once validated the estimates of the free surface elevation based on high frequency GNSS measurements, these estimates were used to characterize the dynamics of the tidal bore

during the 22 s of valid acquisitions. Figure 5 presents the spatio-temporal variations of the three components of the position (x,y,z) of the GNSS antenna during the tidal bore that occurred on the 31st of August 2015 in the Gironde/Garonne estuary.
The tidal passage not only caused an important change on the vertical direction, but also on the horizontal ones. Due to the orientation of the stream in this area of the Garonne River (Fig. 5a), larger variations on the position of the rover antenna can be observed in the north-south direction than east-west one during the passage of the waves (Fig. 5b). Complete changes in direction but of small intensity can be observed before and at the end of the three waves detected during the acquisition period.

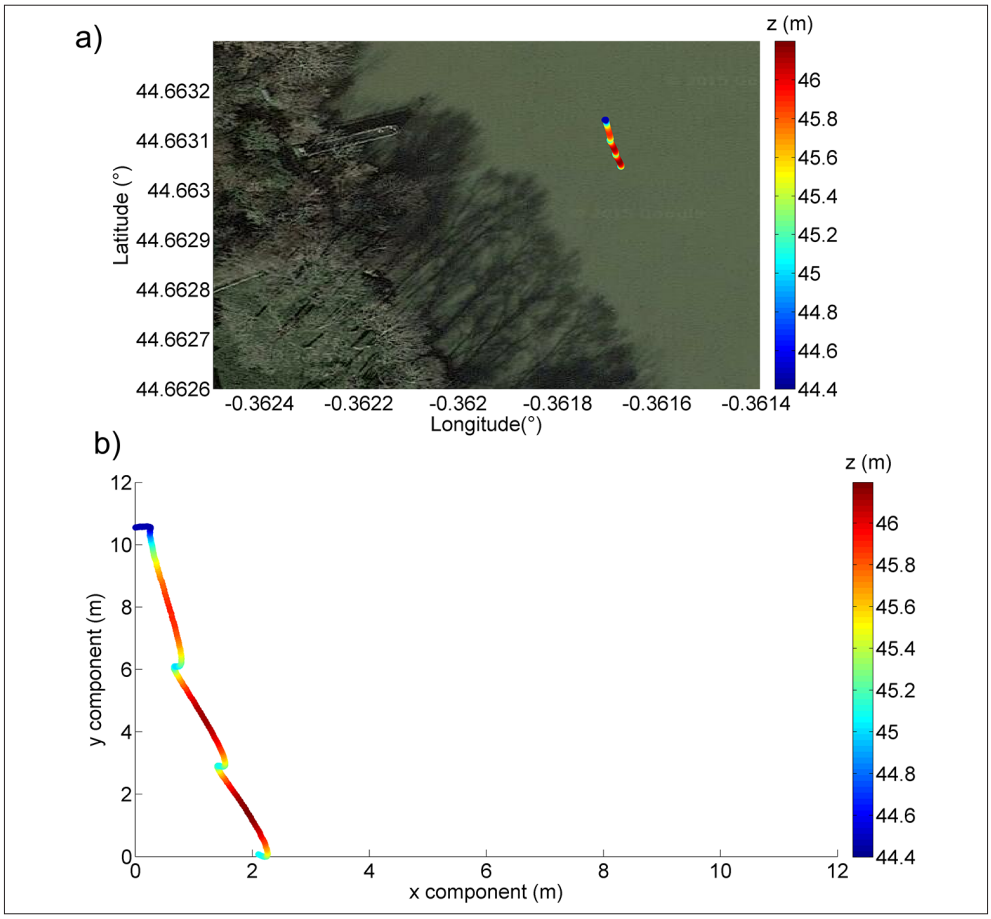

Figure 5 - Spatio-temporal variations of the three components of the position (x,y,z) of the GNSS antenna during the tidal bore, on a satellite image from Google Map © (a), and on a zoom (b).

Changes in position reached 2.30 m in the east-west direction (Fig. 6a), and more than 10 m in the north-south direction (Fig. 6b). They were of increasing amplitude with each tidal bore wave (0.60 m, 0.80 m and 0.90 m respectively) in the east-west direction, and of

decreasing amplitude (4.50 m, 3.30 m and 2.80 m respectively) in the east-west direction (Figs. 6a and 6b).

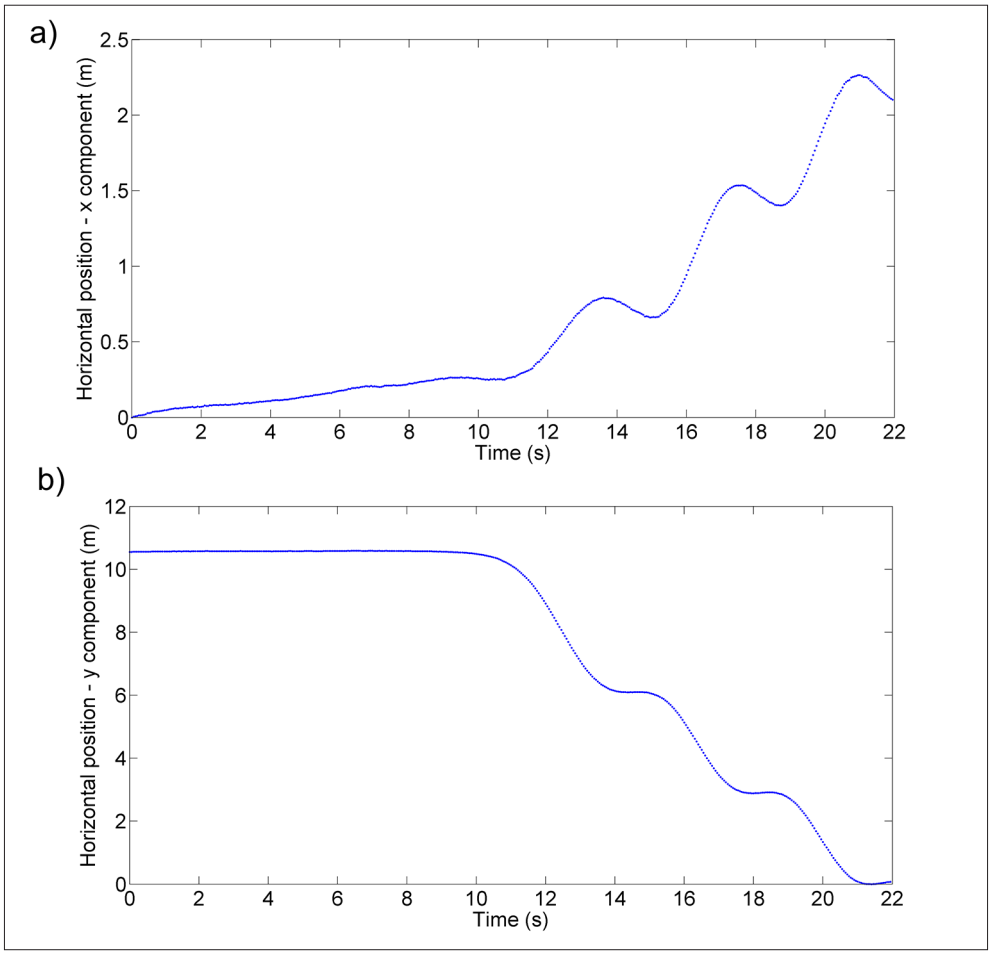

Figure 6 - Time variations of the horizontal components of the position (x,y) of the GNSS antenna during the tidal bore (a and b respectively).

The corresponding horizontal velocities are presented in Figures 7a and 7b for east-west and north-south components. Before the passage of the tidal bore, the GNSS antenna on the top of the buoy was quasi-static. Then, they exhibited almost sinusoidal velocity patterns of modulated amplitudes in both directions. They ranged from -0.2 m.s-1 to 0.4 and 0.6 m.s-1 in the east-west directions (Fig. 7a) and from -2.0 m.s-1 to 0.2 m.s-1 in the north-south directions (Fig. 7b).

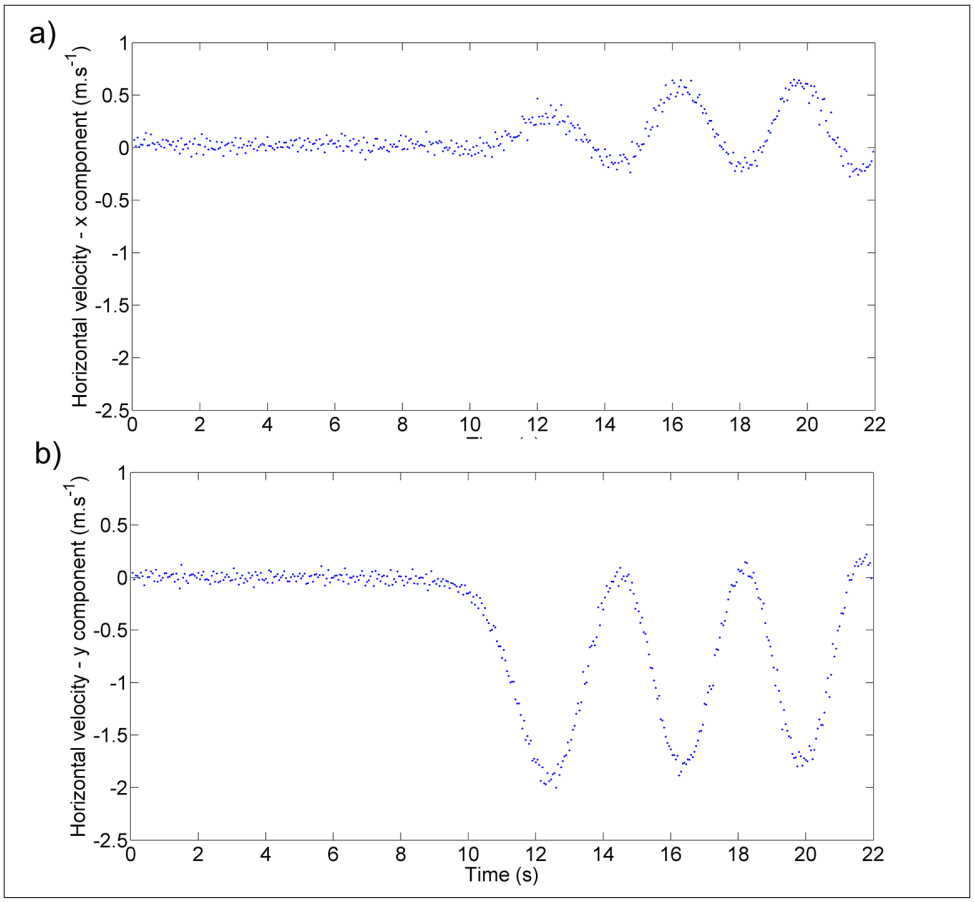

Figure 7 - Time variations of the horizontal components of the velocity of the GNSS antenna during the tidal bore (a and b respectively).

Conclusion

This study demonstrates the strong potential of high frequency GNSS measurements for the monitoring of transitory physical phenomenon such as the nonhydrostatic tidal bore. Here, we used a GNSS receiver and its antenna to monitor a well-developed undular tidal bore that occurred in the Gironde/Garonne estuary on the 31st of August 2015 during spring tide. GNSS-based elevation of the free surface using GPS and GLONASS data provides realistic estimates of the tidal bore amplitude (1.34 m for the first wave) and period (3.0 s) that were in good agreement with values obtained using ADCP measurements. But, due to changes in attitude of the buoy caused by the tidal bore waves, differences up to 10 cm were observed between GNSS and ADCP derived river stages. Besides, as the GNSS buoy drifted during the campaign, valuable information on the dynamics of the tidal bore were estimated (horizontal positions and velocities) that cannot be obtained using moored sensors. But, due to the rapid dynamics of the tidal bore (period of 3.0 s), the GNSS antenna experienced attitude problems that were responsible of 0.05 m to 0.10 m of inaccuracy on the free surface elevation determination.

Acknowledgements

The authors want to thank two anonymous reviewers for their constructive comments that helped us in improving the quality of our manuscript. This work was partly funded by RTRA STAE PRISM project and H2020 MISTRALE project.

References

Apel H., Hung N., Thoss H., Schöne T. (2011) - *GPS buoys for stage monitoring of large rivers*. Journal of Hydrology, 412-413: 182-192. doi: https://doi.org/10.1016/j.jhydrol.2011.07.043.

Avallone A., Marzario M., Cirella A., Piatanesi A., Rovelli A., Di Alessandro C., D'Anastasio E., D'Agostino N., Giuliani R., Mattone M. (2011) - *Very high rate (10 Hz) GPS seismology for moderate-magnitude earthquakes: The case of the Mw 6.3 L'Aquila (central Italy) event*. Journal of Geophyical Research, 116: B02305. doi: http://dx.doi.org/10.1029/2010JB007834.

Avallone A., D'Anastasio E., Serpelloni E., Latorre D., Cavaliere A., D'Ambrosio C., Del Mese S., Massucci S., Cecere G. (2012) - *High-rate (1 Hz to 20 Hz) GPS coseismic dynamic displacements carried out during the Emilia 2012 seismic sequence.* Annals of Geophysics, 55 (4):773-779. doi: http://dx.doi.org/10.4401/ag-6162.

Bender III L.C., Guinasso Jr. N.L., Walpert J.N., Howden S.D. (2010) - *A Comparison of Methods for Determining Significant Wave Height-Applied to a 3-m Discus Buoy during Hurricane Katrina*. Journal of Atmospheric and Oceanic Technology, 27: 1012-1028. doi: http://dx.doi.org/10.1175/2010JTECHO724.1.

Bonnefond P., Laurain O., Exertier P., Guillot A., Picot N., Cancet M., Lyard F. (2015) - *SARAL/AltiKa absolute calibration from the multi-mission Corsica facilities.* Marine Geodesy, 38 (S1): 171-192. doi: http://dx.doi.org/10.1080/01490419.2015.1029656.

Bonneton P., Van de Loock J., Parisot J.-P., Bonneton N., Sottolichio A., Detandt G., Castelle B., Marieu V., Pochon N. (2011) - *On the occurrence of tidal bores-The Garonne River case*. Journal of Coastal Research, SI 64: 11.462-11.466.

Bonneton N., Bonneton P., Parisot J.-P., Sottolichio A., Detandt G. (2012) - *Tidal bore and Mascaret - Example of Garonne and Seine Rivers*. Comptes Rendus Geoscience, 344: 508-515. doi: https://doi.org/10.1016/j.crte.2012.09.003.

Bonneton P., Bonneton N., Parisot J.-P., Castelle B. (2015) - *Tidal bore dynamics in funnel-shaped estuaries*. Journal of Geophysical Research Oceans, 120: 923-941. doi: http://dx.doi.org/10.1002/2014JC010267.

Bouin M.N., Ballu V., Calmant S., Boré J.M., Folcher E., Ammann J. (2009) - *A kinematic GPS methodology for sea surface mapping, Vanuatu*. Journal of Geodesy, 83 (12): 1203-1217. doi: http://dx.doi.org/10.1007/s00190-009-0338-x.

Chanson H., Reungoat D., Simon B., Lubin P. (2011) - *High-frequency turbulence and suspended sediment concentration measurements in the Garonne River tidal bore*. Estuarine and Coastal Shelf Science, 95 (2): 298-306. doi: https://doi.org/10.1016/j.ecss.2011.09.012.

Elósegui P., Davis J.L., Oberlander D., Baena R., Ekström G. (2006) - *Accuracy of high-rate GPS for seismology*. Geophysical Research Letters, 33 (11): L11308. doi: http://dx.doi.org/10.1029/2006GL026065.

Falck C., Ramatschi M., Subarya C., Bartsch M., Merx A., Hoeberechts J., Schmidt G.

(2010) - *Near real-time GPS applications for tsunami early warning systems*. Natural Hazards and Earth System Sciences, 10: 181-189. doi: http://dx.doi.org/10.5194/nhess-10-181-2010.

Frappart F., Roussel N., Biancale R., Martinez Benjamin J.J., Mercier F., Pérosanz F., Garate Pasquin J., Martin Davila J., Perez Gomez B., Gracia Gomez C., Lopez Bravo R., Tapia Gomez A., Gili Ripoll J., Hernandez Pajares M., Salazar Lino M., Bonnefond P., Valles Casanova I. (2015) - *The 2013 Ibiza calibration campaign of Jason-2 and Saral altimeters*. Marine Geodesy, 38 (S1): 219-232. doi: http://dx.doi.org/10.1080/01490419.2015.1008711.

Fund F., Perosanz F., Testut L., Loyer S. (2013) - *An integer precise point positioning technique for sea surface observations using a GPS buoy*. Advances in Space Research, 51 (8): 1311-1322. doi: https://doi.org/10.1016/j.asr.2012.09.028.

Furgerot L., Mouaze D., Tessier B., Perez L., Haquin S. (2013) - *Suspended sediment concentration in relation to the passage of a tidal bore (See River estuary, Mont Saint Michel Bay, NW France)*. Proceedings of Coastal Dynamics 2013, Arcachon, pp. 671-682.

Hofmann-Wellenhof B., Lichtenegger H., Wasle E. (2008) - *GNSS - Global Navigation Satellite Systems - GPS, GLONASS, Galileo, and more*. Springer Science & Business Media, Wien, New York, pp. 518.

IERS Conventions (2010) - *Technical Note 36*. Petit G., Lunzum B. (Eds.).

Montenbruck O., Schmid R., Mercier F., Steigenberger P., Noll C., Fatkulin R., Kogure S., Ganeshan A.S. (2015) - *GNSS satellite geometry and attitude models*. Advances in Space Research, 56 (6): 1015-1029. doi: http://dx.doi.org/10.1016/j.asr.2015.06.019.

Petovello M.G. (2011) - *Differencing the differences: How does measurement differencing affect my computed position?* Inside GNSS Magazine, 6 (5): 28-32.

Remondi B.W. (1985) - *Performing Centimeter-Level Surveys in Seconds with GPS Carrier Phase: Initial Results*. Navigation, 32 (4): 386-400. doi: https://doi.org/10.1002/j.2161-4296.1985.tb00918.x.

Saastamoinen J. (1973) - *Contributions to the theory of atmospheric refraction, part II*. Bulletin Géodésique, 107: 13-34. doi: https://doi.org/10.1007/BF02522083.

Simpson J.H., Fisher N.R., Wiles P. (2004) - *Reynolds stress and TKE production in an estuary with a tidal bore*. Estuarine and Coastal Shelf Science, 60 (4): 619-627. doi: https://doi.org/10.1016/j.ecss.2004.03.006.

Takasu T. (2009) - *RTKLIB: Open source program package for RTK-GPS*. Proceedings of the FOSS4G 2009.

Takasu T., Yasuda A. (2009) - *Development of the low-cost RTK-GPS receiver with an open source program package RTKLIB*. Proceedings of the International Symposium on GPS/GNSS, Jeju, Korea, pp. 4-6.

Uncles R.J., Stephens J.A., Law D.J. (2006) - *Turbidity maximum in the macrotidal, highly turbid Humber Estuary, UK: Flocs, fluid mud, stationary suspensions and tidal bores*. Estuarine and Coastal Shelf Science, 67: 30-52. doi: https://doi.org/10.1016/j.ecss.2005.10.013.

Wolanski E., Williams D., Spagnol S., Chanson H. (2004) - Undular tidal bore dynamics in the Daly Estuary, Northern Australia. Estuarine and Coastal Shelf Science, 60 (4): 629-636. doi: https://doi.org/10.1016/j.ecss.2004.03.001.

Yamagiwa A., Hatanaka Y., Yutsudo T., Miyahara B. (2006) - *Real time capability of GEONET system and its application to crust monitoring.* Bulletin of the Geographical Survey Institute, 53: 27-33.